Research Article | Vol. 12, No. 7 / 1 July 2021 / Biomedical Optics Express 4560
Biomedical Optics EXPRESS

Polarization and depolarization metrics as optical markers in support to histopathology of *ex vivo* colon tissue

DEYAN IVANOV,[1,2,*] VIKTOR DREMIN,[3,4] EKATERINA BORISOVA,[2] ALEXANDER BYKOV,[5] TATIANA NOVIKOVA,[1] IGOR MEGLINSKI,[4,5,6,7,8] AND RAZVIGOR OSSIKOVSKI[1,8]

[1]*LPICM, CNRS, Ecole Polytechnique, Institut Polytechnique de Paris, Palaiseau, France*
[2]*Institute of Electronics, Bulgarian Academy of Sciences, Sofia, Bulgaria*
[3]*Research and Development Center of Biomedical Photonics, Orel State University, Russia*
[4]*College of Engineering and Physical Sciences, Aston University, Birmingham, UK*
[5]*Optoelectronics and Measurement Techniques unit, University of Oulu, Finland*
[6]*Institute of Clinical Medicine N.V. Sklifosovsky, I. M. Sechenov First Moscow State Medical University, Moscow, Russia*
[7]*V. A. Negovsky Scientific Research Institute of General Reanimatology, Federal Research and Clinical Center of Intensive Care Medicine and Rehabilitology, Moscow, 107031, Russia*
[8]*Senior co-authors*
[*]*Correspondence: deyan.ivanov@polytechnique.edu*

Abstract: Tissue polarimetry holds great promise to improve the effectiveness of conventional cancer diagnostics and staging, being a fast, minimally invasive, and low-cost optical technique. We introduce an enhanced diagnostic method for *ex vivo* colon specimens assessment by utilizing Stokes and Mueller matrix polarimetry. The proposed method makes use of experimental Mueller matrices, measured from healthy and tumor zones of a colon specimen, as input data for post-processing algorithms that include physical realisability filtering, symmetric decomposition and estimation of various polarization and depolarization metrics for colon specimen diagnostics. We validated our results with the gold standard histological diagnostics provided by pathologists. It was found that the Stokes-Mueller matrix polarimetry, combined with the appropriate filtering, decomposition algorithms and polarization/depolarization metrics calculations provides relevant optical markers of the colon tissue pathological conditions (healthy versus cancer), as confirmed by histopathology analysis. This approach potentially provides physicians with valuable and complementary information that holds promises in helping with the diagnostics of colon tissue specimens.

1. Introduction

Cancer is one of the most socially significant health problems nowadays and its early theranostics is vital in order to increase life expectancy [1,2]. According to the data from *The Global Cancer Observatory* [3], in 2020 19.3 M of total tumor cases were reported worldwide; out of them 9.96 M ended with mortality. In 2040 the total number of tumor cases is estimated to grow up to 30.2 M with an expected mortality of 16.3 M [3]. Colorectal cancers are in the leading position in terms of incidence and mortality. Contrary to the cancer of skin, the cancer of colon is often detected at the advanced stages due to its anatomical location out of direct sight of view. Therefore, multiple endoscopic tests and biopsy examinations are required for early diagnosis of cancer of the digestive system. For these particular reasons, biophotonics can provide an adequate assistance [4–6].

Tissue polarimetry is a non-invasive, optical diagnostic technique that exploits the extreme sensitivity of optical polarization to early changes in tissue morphology, induced by the malignancy,

#426713 https://doi.org/10.1364/BOE.426713
Journal © 2021 Received 1 Apr 2021; revised 27 May 2021; accepted 29 May 2021; published 30 Jun 2021

Biomedical Optics EXPRESS

without using any contrast agents [4–23]. Any polarization properties of biological tissues affecting both the polarization state of the incident light beam and its degree of polarization (DOP) can be characterised by the transfer function of the optical medium, known as 4×4 Mueller matrix (MM) [24]. However, not every real-valued 4×4 matrix can be considered as a Mueller matrix, since the input Stokes vector of the incident light that is modified by the transfer function should be transformed into an output Stokes vector with a degree of polarization less or equal to 1 [25]. Furthermore, physically realizable, depolarizing MMs must be representable as weighted averages of non-depolarizing MMs, i.e. MMs preserving the DOP of totally polarized input light. Due to measurement errors and noise, this condition may not be met. Such matrices need to undergo a physical realizability filtering, according to the method proposed by Cloude [25,26]. A direct quantitative representation of the optical properties of the sample, derived from its Mueller matrix elements, is possible for homogeneous media only. This is typically not the case with biological samples that are heterogeneous and anisotropic, thus exhibiting a complex dependence of their Mueller matrix elements on their optical properties [27]. For this particular reason, a decomposition algorithm should be implemented – usually the polar decomposition of Lu and Chipman [28] or the symmetric decomposition (SD) [24,29]. Both algorithms of non-linear data compression allow for extracting information on depolarization, diattenuation and retardance of the sample under study. However, the SD of a Mueller matrix is better suited angular-resolved measurements that are commonly used in materials science [30,31]. For instance, SD may provide better representation of the polarization and depolarization phenomena for reflection geometry, by placing a MM of pure/canonical depolarizer between MMs of retardars and diattenuators. To the best of our knowledge, few reports are available on using the SD for the analysis of the polarimetric properties of biological tissues [32,33] or in biomedical applications [23]. In addition, more detailed information on the tissue depolarizating properties can be extracted by calculating the various depolarization parameters and constructing the corresponding depolarization spaces [34–36]. The above mentioned data processing algorithms hold promise in providing quantitative criteria for the discrimination between healthy and pathological tissue zones that are linked to the micro-structure of tissue.

We start by presenting an indirect method for measuring the full Mueller matrix of a sample with a Stokes polarimeter and then apply this method to measure polarimetrically both healthy and malignant zones of thick formalin-fixed colon specimen at oblique incidence. A combined data processing algorithm including physical realizability filtering, symmetric decomposition and calculation of various depolarization metrics from the Mueller matrix was implemented for processing of the experimental data of the colon specimen. Both healthy and cancerous zones of the colon specimen were analyzed in terms of their polarization and depolarization properties calculated with the algorithm. Next, we constructed the 3D canonical, natural, and indices of polarimetric purity (IPP) depolarization spaces and plotted all polarization and depolarization parameters for both healthy and cancerous zones of colon measured at different points. The depolarization parameters for healthy and cancer colon tissue form distinct clusters. The results provide better insight into the structural modifications caused by cancer and suggest using this approach for the optical diagnostics of colon specimens.

2. Theory

First, we define four input polarization states of a light beam characterized by their normalized ($S_0 = 1$) Stokes vectors : $\mathbf{S_{Hi}} = (1, 1, 0, 0)^{\mathrm{T}}, \mathbf{S_{Vi}} = (1, -1, 0, 0)^{\mathrm{T}}, \mathbf{S_{Pi}} = (1, 0, 1, 0)^{\mathrm{T}}$ and $\mathbf{S_{RCi}} = (1, 0, 0, 1)^{\mathrm{T}}$. The respective output Stokes vectors (also normalized), resulting from probing an arbitrary sample with the above input polarized light beams, can be measured with a Stokes polarimeter: $\mathbf{S_{Ho}}, \mathbf{S_{Vo}}, \mathbf{S_{Po}}$ and $\mathbf{S_{RCo}}$. The subscripts denote horizontal linear (H), vertical linear (V), +45 linear (P), and right-circular (RC) polarization states; i – stands for the input states, o – for the output states and the superscript T is for transposition. The input and output Stokes

Biomedical Optics EXPRESS

vectors are connected by the relation $\mathbf{S_o}=\mathbf{M}\cdot\mathbf{S_i}$ [24,29,37] where $\mathbf{M}$ is the Mueller matrix of the sample under measurement. An important relation between Stokes vector elements accounting for the potential presence of depolarization is given by [24,29,37]:

$$S_0 > (S_1^2 + S_2^2 + S_3^2)^{1/2} = \rho \cdot S_0. \tag{1}$$

By knowing the total degree of polarization ρ and the detected signal power $\wp$, the normalized output Stokes vectors reads:

$$\mathbf{S}_{\text{dep}} = \wp \cdot \rho \cdot (S_0 \cdot \rho^{-1}, S_1, S_2, S_3)^T. \tag{2}$$

The four output Stokes vectors $\mathbf{S}_{\text{dep}}$ can be represented as algebraic sums of the columns $\mathbf{C}_l (l = 1, \ldots, 4)$ of the sample Mueller matrix as follows:

$$\mathbf{S_{dep}^H} = \mathbf{C}_1 + \mathbf{C}_2, \quad \mathbf{S_{dep}^V} = \mathbf{C}_1 - \mathbf{C}_2, \quad \mathbf{S_{dep}^P} = \mathbf{C}_1 + \mathbf{C}_3, \quad \mathbf{S_{dep}^{RC}} = \mathbf{C}_1 + \mathbf{C}_4, \tag{3}$$

where all superscripts in Eq. (3) denote the respective input polarization states. By measuring the output Stokes vector for each one of the four different input polarization states, all columns of the Mueller matrix $\mathbf{C}_l$ and therefore, the complete Mueller matrix, can be derived [38]:

$$\mathbf{C}_1 = \frac{\mathbf{S_{dep}^H} + \mathbf{S_{dep}^V}}{2}, \quad \mathbf{C}_2 = \frac{\mathbf{S_{dep}^H} - \mathbf{S_{dep}^V}}{2}, \quad \mathbf{C}_3 = \mathbf{S_{dep}^P} - \mathbf{C}_1, \quad \mathbf{C}_4 = \mathbf{S_{dep}^{RC}} - \mathbf{C}_1. \tag{4}$$

Biological tissues are typically depolarizing media [39] and can be generally characterized by their ability to change both the initial polarization state of the probing beam and its degree of polarization. The former is affected by both (surface) Fresnel reflection and (volume) sample anisotropy whereas the latter is due to the coherence loss resulting from the light-tissue interaction taking the form of multiple scattering events, originating from macroscopic spatial fluctuations of the refractive index. In order to extract both polarization and depolarization properties of a given biological specimen, the symmetric decomposition of the Mueller matrix of the sample can be applied [24,29]:

$$\mathbf{M}=\mathbf{M_{D_2}}\mathbf{M_{R_2}}\mathbf{M_\Delta}\mathbf{M_{R_1}}\mathbf{M_{D_1}}, \tag{5}$$

where the canonical forms of $\mathbf{M}_\Delta, \mathbf{M_R}$ and $\mathbf{M_D}$ is defined as:

$$\mathbf{M}_\Delta = diag(1, d_1, d_2, d_3), \quad \mathbf{M_R} = \begin{bmatrix} 1 & \vec{\mathbf{0}}^{\mathbf{T}} \\ \vec{\mathbf{0}} & \mathbf{m}_\varphi \end{bmatrix}, \quad \mathbf{M_D} = \begin{bmatrix} 1 & \vec{\mathbf{D}}^{\mathbf{T}} \\ \vec{\mathbf{D}} & \mathbf{m_D} \end{bmatrix}. \tag{6}$$

In Eq. (6), $\mathbf{M}_\Delta$ describes a diagonal depolarizer of type I [24] with depolarization coefficients $d_i (i = 1, \ldots, 3)$, where subscript 1 denotes depolarization of H and V linear polarization, subscript 2 - of $\pm 45^\circ$ linear polarization and subscript 3 - of right and left circular polarization states, respectively. $\mathbf{M_R}$ and $\mathbf{M_D}$ denote respectively the Mueller matrices of a (general elliptical) retarder and a diattenuator. The 3×3 submatrix $\mathbf{m}_\varphi$ is 3D rotation matrix through the angle specified by the phase shift or retardance φ, whereas the 3×3 submatrix $\mathbf{m_D}$ is constructed from the diattinuation $\vec{\mathbf{D}}$. Finally, the net depolarization Δ, diattenuation D, polarizance P and retardance φ can be expressed as [24]:

$$\Delta = 1 - \frac{|d_1| + |d_2| + |d_3|}{3}, \quad 0 \le \Delta \le 1, \tag{7a}$$

$$D = \frac{1}{M_{11}} \left[\sum_l M^2{}_{1l} \right]^{1/2}, \quad l = 2, 3, 4, \quad 0 \le D \le 1, \tag{7b}$$

Biomedical Optics EXPRESS

$$P = \frac{1}{M_{11}}\left[\sum_{k} M^2{}_{k1}\right]^{1/2}, \quad k = 2,3,4, \quad 0 \le P \le 1, \tag{7c}$$

$$\varphi = \arccos\left[\frac{tr(\mathbf{m}_\varphi) - 1}{2}\right]. \tag{7d}$$

Next, each Mueller matrix can be cast into the form of the so called covariance matrix **H**, a Hermitian matrix defined as [34–36]:

$$\mathbf{H} = \frac{1}{4}\sum_{k,l=1}^{4} M_{\mathrm{kj}}(\sigma_{\boldsymbol{k}} \otimes \sigma_{\boldsymbol{l}}), \tag{8}$$

where $\sigma_{\mathbf{k}}$ are the four Pauli spin matrices and the symbol $\otimes$ denotes the Kronecker product. [25] The eigenvalues of the matrix **H**, arranged in decreasing order ($\lambda_1 \ge \lambda_2 \ge \lambda_3 \ge \lambda_4$), are used to derive the indices of polarimetric purity (IPP) [34–36,40,41]:

$$P_1 \equiv \frac{\lambda_1 - \lambda_2}{tr\mathbf{H}}, \quad P_2 \equiv \frac{\lambda_1 + \lambda_2 - 2\lambda_3}{tr\mathbf{H}}, \quad P_3 \equiv \frac{\lambda_1 + \lambda_2 + \lambda_3 - 3\lambda_4}{tr\mathbf{H}}, \tag{9}$$

where *tr* denotes the trace of a matrix. It is known that high concentrations of scattering particles and/or high structural sample anisotropy enhance the scattering of light and, consequently, the depolarization effect. [26] According to the values of the indices of polarimetric purity $P_i (i = 1, \ldots, 3)$, there are two limiting cases: ideal depolarizing medium when $P_i = 0$ and a non-depolarizing one when $P_i = 1$. From the IPP values one can calculate the polarimetric purity index *PI* and the Gil-Bernabeu's depolarization index P_Δ likewise [42]:

$$PI = \left[\frac{1}{3}(P_1^2 + P_2^2 + P_3^2)\right]^{1/2}, \quad P_\Delta = \left[\frac{1}{3}(2P_1^2 + \frac{2}{3}P_2^2 + \frac{1}{3}P_3^2)\right]^{1/2}. \tag{10}$$

At this point, it is practical to draw a parallel between the extrinsic and intrinsic depolarization parameters of a given **M**. The former are described by the eigenvalues of the covariance matrix **H** associated with **M** whereas the latter are defined by the eigenvalues of the covariance matrix $\mathbf{H}_\Delta$ of the canonical depolarizer $\mathbf{M}_\Delta$. In the absence of diattenuation the matrices of both diattenuators in the symmetric decomposition are equal to the identity matrix and the extrinsic and intrinsic depolarization parameters are equal. Otherwise, the diattenuators have the capability to alter the degree of polarization of partially polarized light by introducing repolarizing effect and thus, making the difference between the two sets of depolarization parameters.

Eventually, by introducing the Cloude's entropy parameter *S* in addition to *PI* and P_Δ, one may enrich the depolarization parameterization. *S* can be calculated from the eigenvalues λ_i of the covariance matrix **H** from the following expression:

$$S = -\sum_{k=1}^{4} \lambda_{\mathrm{k}} log_4(\lambda_{\mathrm{k}}). \tag{11}$$

The value of $S = 1$ corresponds to an ideal depolarizer (i.e. $\lambda_1 = \lambda_2 = \lambda_3 = \lambda_4$); the respective turbid medium exhibits polarimetric properties that fluctuate completely at random. Conversely, a turbid medium with $S = 0$ is a non-depolarizing one, i.e. it completely preserves the degree of polarization of totally polarized light [29].

3. Sample preparation

A formalin-fixed human colon specimen was used for *ex vivo* polarimetric measurements (see Fig. 1). The tissue specimen was provided in the framework of a cooperation agreement for optical

Biomedical Optics EXPRESS

investigations of cancerous tissues between the Institute of Electronics – Bulgarian Academy of Sciences and the Surgical Department of University Hospital "Tsaritsa Yoanna – ISUL", Sofia under approval #286/2012 of the local Ethical Committee. After a surgical excision procedure, the biological specimen was cut into two parts for histological and optical examination, where the tumor staging was performed by the pathologist. The histology analysis confirmed the presence of a tumor zone containing G2-adenocarcinoma (T2, N0, M0) [43] with moderately differentiated tumor cells. No spread to regional lymph nodes was found. However, the tumor had grown into the *muscularis propria* layer of colon wall. Thus, the results of the histological examination were used as a "gold standard" and reference to polarimetric diagnostic measurements. Both healthy and tumor zone thicknesses were about 1 mm; therefore, the polarimetric measurements were done in reflection configuration.

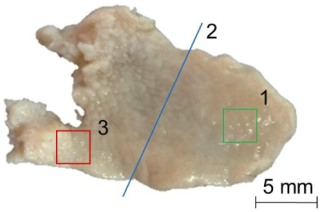

Fig. 1. *Ex vivo* colon specimen used for measurements. All of the following zones were annotated by the pathologist. Green square – 1) marks the site within which the healthy ROI corresponds, blue line – 2) separates the two adjacent tissue zones and the red square – 3) marks the site within which the tumor ROI corresponds.

4. Experimental setup and data processing algorithms

In order to measure the full Mueller matrix, at least sixteen independent measurements have to be conducted with different polarization states generated by the polarization state generator (PSG) and analyzed by the polarization state detector (PSD) channels of the polarimetric equipment. Instead of using discrete polarization states, one may use continuous polarization modulation, typically achieved either with liquid crystal retarders or with rotating wave-plates. In our work, the PSG polarization states were set discretely, while those of the PSD were modulated continuously, thus reducing the number of discrete measurements to only four. In Fig. 2 the PSG and PSD channels are presented in a side view for better clarity. All optical elements were inserted in tube systems, in order to block stray light that could interfere with the probing or detected beam. The field of view (FoV) of the system was found to be 100×100 μm. In the reflection geometry used, the angles of incidence and detection were respectively set to 55° and 30°. Such configuration was found earlier [23] to enrich the polarimetric response of the turbid medium and is good to be combined with the SD. By this way the off-diagonal MM elements are non-zero and the final form of the MM is different from diagonal depolarizer. For instance, in [18] Pierangelo et al. used normal detection for the backscattered photons and the experimental MM at 600 nm bares strong resemblance to diagonal depolarizer. Additionally, Nishizawa et al. have also reported valuable angular optimizations for tissue polarimetric measurements in [44].

For our experiments, a supercontinuum fiber laser – SC (Leukos Ltd., France), connected to an acousto-optic tunable filter – AOTF (Leukos Ltd., France), generated the selected measurement wavelength of 635 nm with a spectral width of 8 nm and output power of 2 mW. Two irises were used to obtain a collimated beam. A half-wave plate was inserted to vary the azimuth of the linearly polarized laser beam, while an electrically-driven liquid crystal variable quarter-wave plate was used to generate circular polarization. By means of the lens L_1 the light beam was focused to a particular depth of the sample volume. Objective lenses with 10× magnification

Biomedical Optics EXPRESS

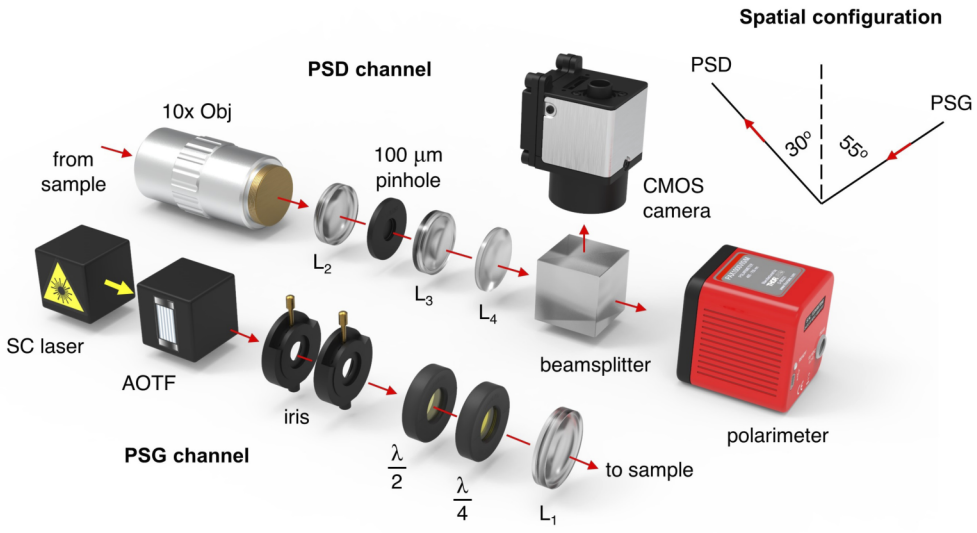

Fig. 2. Schematic representation of the experimental setup.

collected the diffusely scattered light, whereas the lens L_2, the 100 μm pinhole and the lens L_3 were employed to eliminate any out-of-focus photons. By using another lens, L_4 , the light was focused onto a 90-10 beam splitter; the reflected beam was detected by a CMOS camera for accurate focus adjustment while the transmitted beam was analyzed by the polarimetric device (Thorlabs Ltd., USA). A rotating quarter-wave plate and a fixed linear polarizer inside the polarimetric device continuously modulate the light beam before it reaches the photo-detector *Si* photodiode. Prior to conducting the experiments with the biological specimen, the optical set-up was tested by measuring a mirror MM ($\mathbf{M}_{\text{exp}}$), which was compared to a theoretical MM of reflection ($\mathbf{M}_{\text{th}}$) without any depolarization properties - i.e. diag(1,1,1,1). Afterwards, a calculation of the *RMSE* for each matrix element, except for m_{11} was performed.

$$\mathbf{M_{th}} = diag(1,1,1,1), \quad \mathbf{M_{exp}} = \begin{bmatrix} 1 & 0.024 & 0.039 & -0.020 \\ 0.010 & 0.938 & -0.002 & 0.004 \\ -0.006 & 0.002 & 0.978 & 0.002 \\ -0.003 & 0.002 & 0.006 & 1.013 \end{bmatrix}, \quad \text{RMSE} = 0.022. \tag{12}$$

By using a motorized translation stage, both healthy and cancer colon zones were scanned independently over the region of interest (ROI) of 1 mm^2 and a step size of 0.2 mm in x-y directions. For each one of the four input polarization state measurements, the degree of polarization ρ of the measured output Stokes vector was calculated and a normalization procedure was applied (see Eq. (2)). A total of 36 Mueller matrices were obtained for all scanning points of each tissue zone (healthy and cancerous) via Eq. (4). All Mueller matrices were tested and filtered in accordance with the physical realizability criterion; as a result, three matrices per tissue zone were discarded from the data set due to non-compliance. The remaining matrices were decomposed using the symmetric decomposition and the depolarization metric calculations were performed. In Eq. 13 an example of MMs for both health conditions ($\mathbf{M_{Hc}}$ and $\mathbf{M_{Tc}}$) in compliance to the Cloude's realizability method are shown. Both remain unchanged after filtration. Similarly, an example of tumor MM ($\mathbf{M_{Tnc}}$) not in compliance to the Cloude's realizability method is shown again in Eq. (13). Additionally, in Eq. (14) the corresponding diagonal matrices are comprised with the eigenvalues from the corresponding covariance matrices of the aforementioned MMs ($\Lambda_{\mathbf{Hc}}$, $\Lambda_{\mathbf{Tc}}$

Biomedical Optics EXPRESS

and $\Lambda_{\mathbf{Tnc}}$). As can be seen, the MM not in compliance has a negative eigenvalue.

$$\mathbf{M_{Hc}} = \begin{bmatrix} 1 & 0.028 & -0.070 & -0.114 \\ 0.042 & 0.019 & 0.003 & -0.009 \\ 0.014 & 0.004 & -0.012 & -0.004 \\ 0.004 & -0.001 & 0.006 & 0.001 \end{bmatrix}, \quad \mathbf{M_{Tc}} = \begin{bmatrix} 1 & 0.152 & 0.064 & -0.101 \\ 0.244 & 0.468 & 0.085 & -0.043 \\ -0.098 & 0.071 & -0.361 & -0.070 \\ 0.019 & -0.010 & 0.065 & -0.287 \end{bmatrix}, \quad \mathbf{M_{Tnc}} = \begin{bmatrix} 1 & 0.218 & 0.487 & 0.422 \\ 0.339 & 0.456 & 0.541 & 0.354 \\ -0.043 & 0.190 & -0.396 & -0.158 \\ 0.008 & -0.009 & 0.089 & -0.389 \end{bmatrix}. \tag{13}$$

$$\Lambda_{\mathrm{Hc}} = \mathrm{diag}(0.299, 0.270, 0.224, 0.207), \quad \Lambda_{\mathrm{Tc}} = \mathrm{diag}(0.569, 0.193, 0.141, 0.098), \quad \Lambda_{\mathrm{Tnc}} = \mathrm{diag}(0.776, 0.172, 0.106, -0.054) \tag{14}$$

In the figures of the following section either scatter or surface plots were generated. For the latter, a linear interpolation between the experimental data points was implemented.

5. Results and discussion

5.1. Polarization metrics and symmetric decomposition

First, we investigated the ability of the net diattenuation D, the polarizance P, and of the two pairs of polarization parameters (D_i and R_i, $i = 1, 2$) from the symmetric decomposition to discriminate the tumor zone of the colon specimen from the healthy one.

Figure 3(a,b) show the scatter plots of D versus P and D_2 versus D_1, respectively. The polarization parameters were calculated from the experimental Mueller matrices for all measurement points. Both plots hold great potential to be considered as diagnostically relevant and to support colon histopathology analysis, because the points that represent two different zones (healthy and cancer) clearly form two distinctive clusters. The diattenuation values are significant for both tissue sections, which justifies the subsequent use of the extrinsic depolarization space. The D_2 parameter demonstrates a larger spread of values for the tumor zone compared to the healthy one, suggesting the use of the D_2 parameter as a decision variable for colon tissue diagnostics. The diagnostic value of the diattenuation was also demonstrated in [12], but the values of the diattenuation were calculated from the Lu-Chipman decomposition. Next, the retardance values demonstrate large spatial fluctuations within both healthy and cancerous zones and cannot provide accurate diagnostic information (see Fig. 3(c)). It is worth to mention that polarimetric experiments on a fresh colon specimen reported low retardance values [18]. Note that the retardance matrices can also be used to calculate the optical activity from the relation: $\tan\psi = [(\mathbf{m}_\varphi(1,2) - \mathbf{m}_\varphi(2,1)) \cdot (\mathbf{m}_\varphi(1,1) + \mathbf{m}_\varphi(2,2))^{-1}]$. In our studies, no optical activity was found within both cancerous and healthy zones of the colon specimen.

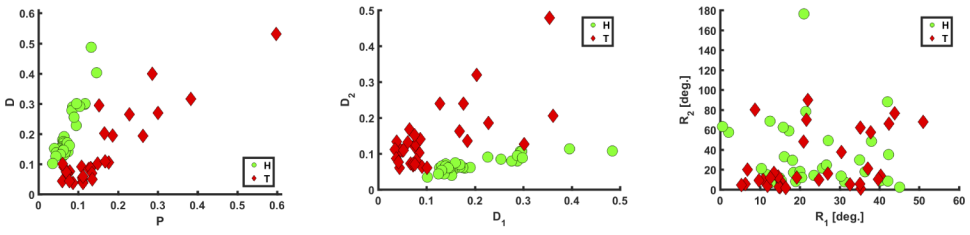

(a) (b) (c)

Fig. 3. Scatter plots of: (a) D vs P, (b) D_2 vs D_1 and (c) R_2 vs R_1, for both health conditions.

Next, we present the 3D spatial plots of both polarizance (P) and output diattenuation (D_2) within the cancerous and the healthy tissue zones since these two polarization parameters exhibit the most distinct polarimetric responses for the two zones.

As can be seen in Fig. 4, both P and D_2 values are very different for the cancerous and the healthy zones of the colon specimen. As the polarimetric measurements were performed at angles of incidence and detection different from the normal to the sample surface, the impact of

Biomedical Optics EXPRESS

surface topography is enhanced. The latter may explain the increased diagnostic value of both P and D_2 parameters which are likely affected by surface and/or volume scattering. Indeed, the colon specimen used in our studies was found to have higher surface roughness within the tumor zone. However, the detailed analysis of the contributions of the surface and volume scattering to the values of P and D_2 polarimetric parameters is beyond the scope of this study and is a subject of future work.

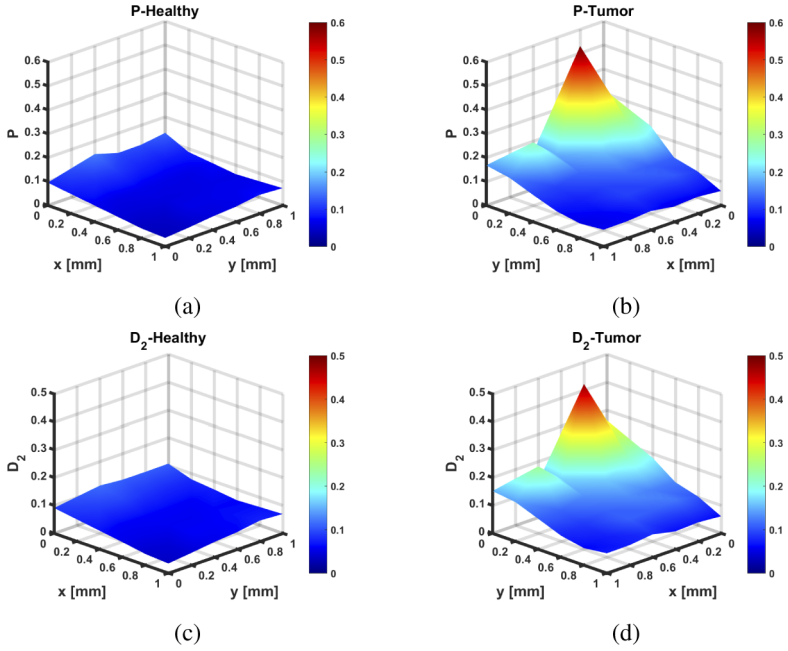

Fig. 4. Spatial distribution of the values of polarizance and diattenuation within both tissue zones: (a) P – Healthy, (b) P – Tumor, (c) D_2 – Healthy, (d) D_2 – Tumor.

Finally, the intrinsic depolarization can be characterized with the spatial distribution of Δ (see Fig. 5). Low values of Δ indicate low depolarization of the probing light by the sample. Tumor tissues are known to be less depolarizing, as the morphological alterations induced by the cancer break the fine complex structure of the healthy tissue and, consequently, decrease light scattering and favor Rayleigh-Mie regime transition [45]. Hence, the low values of Δ can be used as an optical indicator of a tumor spread throughout the scanned tissue zone.

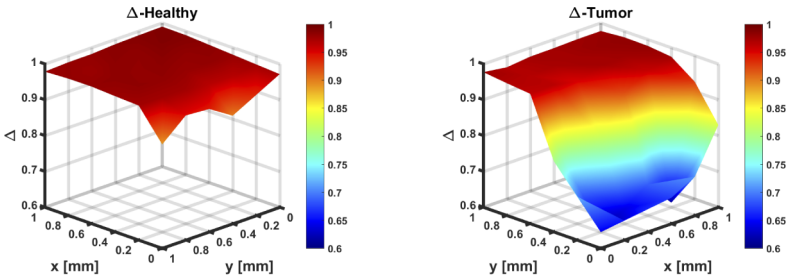

Fig. 5. Spatial distribution of the depolarization Δ within the scanned tissue zones: (a) Δ – Healthy, (b) Δ – Tumor.

Biomedical Optics EXPRESS

5.2. Depolarization metrics

We likewise analyzed our experimental data by using various depolarization metrics and the relevant depolarization spaces.

Upon structural modifications in tissues due to malignancy, an alteration of the ECM is followed by destruction of the collagen cross-links. Also, the effective size of the comprising scattering particles is changed too [46,47]. Thus, both the polarization and depolarization properties of tissues are inevitably affected when tumors are developing. For this particular reason, an indirect measurement of the polarization entropy S could be regarded as a representative quantity of the tissue spatial heterogeneity. Fig. 6 reveals a lower entropy for the cancer zone in comparison to the healthy tissue zone. Specifically, the same spatial location within the cancerous zone is characterized by both lower depolarization Δ from Fig. 5 and lower entropy S. Hence, the polarization entropy S can be a good diagnostic indicator of the sample inner structure arrangement and organization. Note that, since S is derived from the eigenvalues of the covariance matrix $\mathbf{H}$, it is directly correlated to P_Δ and PI. In fact, all three depolarization parameters belong to the extrinsic depolarization space. Conversely, the relation between S and Δ is a complex indirect one because Δ is an intrinsic depolarization space parameter.

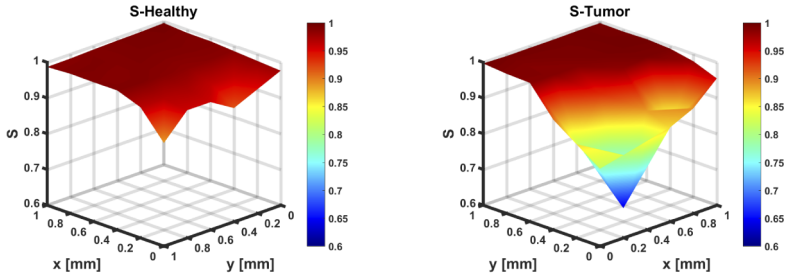

(a) (b)

Fig. 6. Spatial distribution of the polarization entropy S within the scanned tissue zones: (a) S – Healthy, (b) S – Tumor.

Even more depolarization information can be extracted by adopting the concept of polarimetric purity [34–36,40,41,48] and by relating the values of the parameters from the extrinsic depolarization space to the health conditions of the tissue samples under study. Thus, Fig. 7 reveals two important features for both histological conditions, namely a higher polarimetric purity and an increased value of P_Δ depolarization index for the tumor tissue zone compared to the healthy one. As a result, the cancerous tissue zone acts as weaker depolarizer compared to the healthy colon tissue, as previously discussed. At this point, a parallel should be drawn between the depolarization Δ and the depolarization index P_Δ. Their interchangeable use should be avoided since these parameters originate from different depolarization spaces. Moreover, as can be seen from Fig. 5 and 7 the same scanned area is characterized by opposite magnitude values of Δ and P_Δ .

It is worth to visualize all 3D depolarization spaces (see Fig. 8), as such representation potentially reinforces the polarimetric support to histopathology. In Fig. 8 there are two sets of points, marked by green and red color, that represent the respective values for cancerous and healthy tissue zones of the parameters belonging to different depolarization spaces (canonical, natural and IPP). One notices that some of the tumor measurements are very closely grouped to the healthy cluster, making these values diagnostically irrelevant. Fortunately, the rest of the tumor data points are grouped separately from the healthy zone ones; they are to be related to the higher polarimetric purity and Gil-Bernabeu depolarization index values in Fig. 7, as well as to the lower depolarization and entropy in Fig. 5 and 6. Hence, these plots enable us to

Biomedical Optics EXPRESS

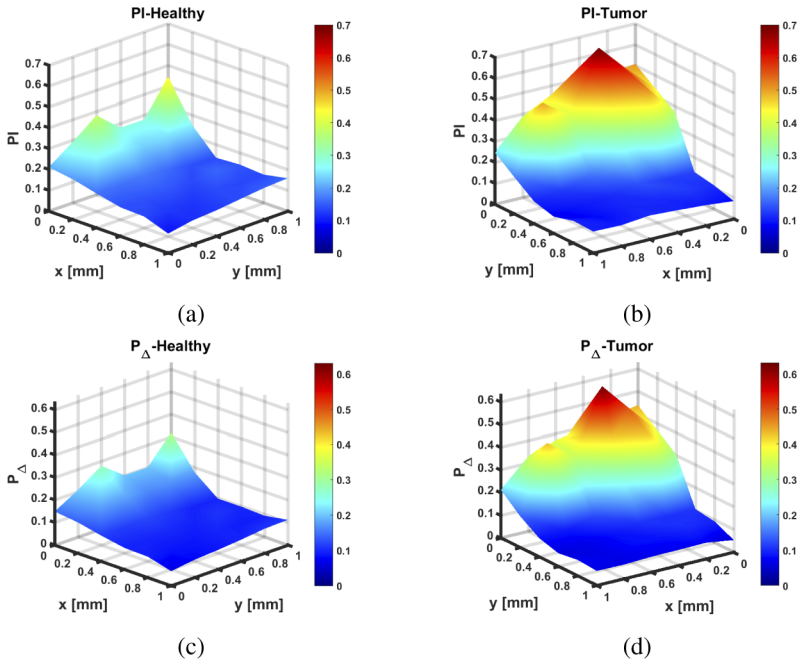

Fig. 7. Spatial distribution of the polarimetric purity – PI and the Gil-Bernabeu's depolarization index – P_Δ within the scanned tissue zones: (a) PI – Healthy, (b) PI – Tumor, (c) P_Δ – Healthy, (d) P_Δ – Tumor.

differentiate the two health conditions, provided there is a significantly decreased depolarization in the corresponding ROI.

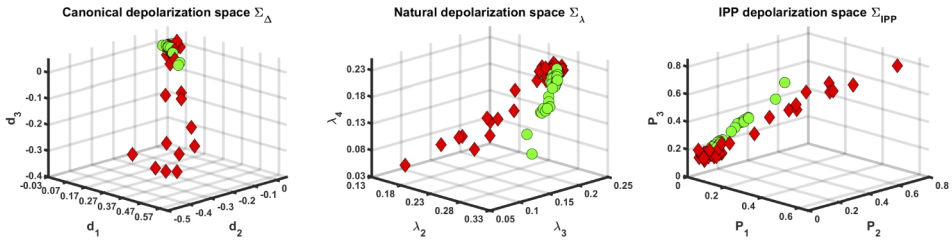

Fig. 8. 3D representation of: (a) Canonical, (b) Natural, (c) Indices of polarimetric purity depolarization spaces, where the symbols represent ○ – Healthy, ◆ – Tumor data points.

6. Conclusions

In our previous work [22], healthy versus tumor differentiation was successfully achieved by tracing changes in the polarization states represented on the surface of the Poincaré sphere. As a logical continuation, in this manuscript the same ROIs were analysed in terms of polarization and depolarization parameters. We believe that both methods could be potentially useful for optical diagnostics and may assist pathologists in colon cancer detection. In this study, we combined both Stokes and Mueller matrix polarimetry to measure the complete MMs of the scanned ROIs of an *ex vivo* colon specimen. In-house algorithm was developed and applied for data post-processing,

Biomedical Optics EXPRESS

matrix filtering and decomposition, as well as for constructing three depolarization spaces for healthy versus tumor differentiation. The physical realizability criterion allowed us to filter our data for noise and experimental errors, before decomposing the experimental MMs from the scanned ROIs. To sum up, the colon specimen exhibits non-negligible polarizance and diattenuation values, determining the separation between external and internal depolarization spaces. From our results, both polarizance and diattenuation can be classified as highly discriminating polarimetric parameters. Moreover, the diattenuation can be employed as a diagnostic quantity, obtained either from its net value or from the symmetric decomposition. Further, no optical activity was found for both tissue sections. All depolarization metrics indicate larger depolarization and higher spatial heterogeneity for the healthy section, while higher polarimetric purity with less depolarization and heterogeneity was revealed for the malignant zone of the colon specimen. It was shown earlier [22,49], that the circular polarization is very sensitive to morphological alterations and provides good opportunities to detect cancer within particular ROIs. However, by measuring and decomposing the full MMs of both health conditions, one is able to add more polarimetric parameters in the analysis, potentially enriching the sample characterization and consequently, enhancing the diagnostic support to colon histopathology. Finally, measuring more colon tissue specimens with different cancer stages, will potentially contribute to building a polarimetric model, performing tissue classification with machine-learning algorithms and providing clinicians with more accurate and advanced polarimetric diagnostics using optical markers in support to colon histopathology.

Funding. Ministry of Science and Higher Education of the Russian Federation (075-15-2020-926); Bulgarian National Science Fund (#KP06-N28/11/14.12.18); Academy of Finland (314369, 325097); ATTRACT (777222); Infotech Oulu.

Acknowledgements. The manuscript is intended to pay special tribute to Assoc. Prof. Ekaterina Borisova, PhD, since, without remorse, COVID-19 pulled out a magnificent scientist from further personal and academic achievements. We, therefore, rightfully commemorate her dedicated and devoted contribution to biophotonics, her readiness to always support, help, motivate and inspire all her colleagues and collaborators. All authors would like to express deepest condolences and sincere support to her family, friends, relatives and colleagues.

Deyan Ivanov acknowledges the PhD fellowship funding by the Doctoral School of Institut Polytechnique de Paris. Special acknowledgements to Dr. Tsanislava Genova and Boyko Kolev for their contribution of this work.

Disclosures. The authors declare no potential conflict of interests.

Data availability. Data underlying the results presented in this paper are not publicly available at this time, due to restrictions for confidentiality reasons.

References

1. O. M. Zaytoun and J. S. Jones, "Prostate cancer detection after a negative prostate biopsy: lessons learnt in the Cleveland Clinic experience," Int. J. Urol. **18**(8), 557–568 (2011).
2. K. Nourish, *Skin Cancer* (The McGraw-Hill Companies Inc., 2008).
3. I. Agency for Research on Cancer, "Global Cancer Observatory: Cancer Today," (2021). Available from: http://gco.iarc.fr [last accessed: March 2021].
4. V. Ushenko, B. Hogan, A. Dubolazov, A. Grechina, T. Boronikhina, M. Grosky, A. Ushenko, Y. Ushenko, A. Bykov, and I. Meglinski, "Embossed topographic depolarisation maps of biological tissues with different morphological structures," Sci. Rep. **11**(1), 3871 (2021).
5. V. Ushenko, B. Hogan, A. Dubolazov, G. Piavchenko, S. Kuznetsov, A. Ushenko, Y. Ushenko, M. Gorsky, A. Bykov, and I. Meglinski, "3D Mueller matrix mapping of layered distributions of depolarisation degree for analysis of prostate adenoma and carcinoma diffuse tissues," Sci. Rep. **11**(1), 5162 (2021).
6. I. Meglinski, L. Trifonyk, V. Bachinsky, O. Vanchulyak, B. Bodnar, M. Sidor, O. Dubolazov, A. Ushenko, Y. Ushenko, I. Soltys, A. Bykov, B. Hogan, and T. Novikova, *Shedding the Polarized Light on Biological Tissues*. (Spinger Briefs in Applied Science and Technology, Springer, Singapore, 2021).
7. B. Kunnen, C. Macdonald, A. Doronin, S. Jacques, M. Eccles, and I. Meglinski, "Application of circularly polarized light for non-invasive diagnosis of cancerous tissues and turbid tissue-like scattering media," J. Biophotonics **8**(4), 317–323 (2015).
8. N. Ghosh and I. Vitkin, "Tissue polarimetry: concepts, challenges, applications, and outlook," J. Biomed. Opt. **16**(11), 110801 (2011).
9. T. Novikova, I. Meglinski, J. C. Ramella-Roman, and V. V. Tuchin, "Special section guest editorial: Polarized light for biomedical applications," J. Biomed. Opt. **21**(7), 071001 (2016).

Biomedical Optics EXPRESS

10. V. T. Bachinskyi, O. Y. Wanchulyak, A. Ushenko, Y. A. Ushenko, A. V. Dubolazov, and I. Meglinski, *Polarization Correlometry of Scattering Biological Tissues and Fluids* (Springer, Singapore, 2020).
11. N. Das, S. Chakraborty, S. Dey, P. Panigrahi, I. Meglinski, and N. Ghosh, "Quantitative assessment of submicron scale anisotropy in tissue multifractality by scattering Mueller matrix in the framework of Born approximation," Opt. Commun. **413**, 172–178 (2018).
12. I. Ahmad, M. Ahmad, K. Khan, S. Ashraf, S. Ahmad, and M. Ikram, "*Ex vivo* characterization of normal and adenocarcinoma colon samples by Mueller matrix polarimetry," J. Biomed. Opt. **20**(5), 056012 (2015).
13. V. Dremin, D. Anin, O. Sieryi, M. Borovkova, J. Näpänkangas, I. Meglinski, and A. Bykov, "Imaging of early stage breast cancer with circularly polarized light," Proc. SPIE **11363**, 1136304 (2020).
14. T. Novikova, A. Pierangelo, S. Manhas, A. Benali, P. Validire, B. Gayet, and A. De Martino, "The origins of polarimetric image contrast between healthy and cancerous human colon tissue," Appl. Phys. Lett. **102**(24), 241103 (2013).
15. M. Kupinski, M. Boffety, F. Goudail, R. Ossikovski, A. Pierangelo, J. Rehbinder, J. Vizet, and T. Novikova, "Polarimetric measurement utility for pre-cancer detection from uterine cervix specimens," Biomed. Opt. Express **9**(11), 5691–5702 (2018).
16. P. Schucht, H. R. Lee, M. H. Mezouar, E. Hewer, A. Raabe, M. Murek, I. Zubak, J. Goldberg, E. Kövari, A. Pierangelo, and T. Novikova, "Visualization of white matter fiber tracts of brain tissue sections with wide-field imaging Mueller polarimetry," IEEE Trans. Med. Imaging **39**(12), 4376–4382 (2020).
17. T. Novikova, J. Rehbinder, H. Haddad, S. Deby, B. Teig, A. Nazac, A. Pierangelo, F. Moreau, and A. De Martino, "Multi-spectral Mueller matrix imaging polarimetry for studies of human tissue," *OSA Biophotonics Congress, Clinical and Translational Biophotonics*, p. TTh3B (2016).
18. A. Pierangelo, S. Manhas, A. Benali, M.-R. Antonelli, T. Novikova, P. Validire, B. Gayet, and A. De Martino, "Use of Mueller polarimetric imaging for the staging of human colon cancer," Proc. SPIE **7895**, 78950E (2011).
19. D. Ivanov, R. Ossikovski, T. Novikova, P. Li, B. Borisova, T. Genova, L. Nedelchev, and D. Nazarova, "Tissue polarimetric study I: In search of reference parameters and depolarazing Mueller matrix model of *ex vivo* colon samples," Proc. SPIE **11075**, 1107514 (2019).
20. D. Ivanov, T. Genova, E. Borisova, L. Nedelchev, and D. Nazarova, "Multiwavelength polarimetry of gastrointestinal *ex vivo* tissues for tumor diagnostic improvement," Proc. SPIE **11047**, 1104707 (2019).
21. D. Ivanov, E. Borisova, T. Genova, L. Nedelchev, and D. Nazarova, "Tissue polarimetric discrimination analysis of skin and colon histological samples," AIP Conf. Proc.. **2075**, 170017 (2019).
22. D. Ivanov, V. Dremin, A. Bykov, E. Borisova, T. Genova, A. Popov, T. Novikova, R. Ossikovski, and I. Meglinski, "Colon cancer detection by using Poincaré sphere and 2D polarimetric mapping of *ex vivo* colon samples," J. Biophotonics **13**(8), e202000082 (2020).
23. D. Ivanov, V. Dremin, E. Borisova, A. Bykov, I. Meglinski, T. Novikova, and R. Ossikovski, "Symmetric decomposition of Mueller matrices reveals a new parametric space for polarimetric assistance in colon cancer histopathology," Proc. SPIE **11646**, 1164614 (2021).
24. D. H. Goldstein, *Polarized Light - Third edition* (CRC Press, 2010).
25. S. Cloude, "Conditions for the physical realizability of matrix operators in polarimetry," Proc. SPIE **1166**, 177–185 (1989).
26. S. Cloude, "Group theory and polarisation algebra," Optik(Stuttgart) **75**, 26–36 (1986).
27. M. Borovkova, M. Peyvasteh, O. Dubolazov, Y. Ushenko, V. Ushenko, A. Bykov, S. Deby, J. Rehbinder, T. Novikova, and I. Meglinski, "Complementary analysis of Mueller-matrix images of optically anisotropic highly scattering biological tissues," J. Eur. Opt. Soc.-Rapid Publ. **14**(1), 20 (2018).
28. S. Y. Lu and R. A. Chipman, "Interpretation of Mueller matrices based on polar decomposition," J. Opt. Soc. Am. A **13**(5), 1106–1113 (1996).
29. J. J. Gil Pérez and R. Ossikovski, *Polarized Light and the Mueller Matrix Approach* (CRC Press, Taylor and Francis, 2016).
30. R. Ossikovski, "Analysis of depolarizing Mueller matrices through a symmetric decomposition," J. Opt. Soc. Am. A **26**(5), 1109–1118 (2009).
31. J. Vizet and R. Ossikovski, "Symmetric decomposition of experimental depolarizing Mueller matrices in the degenerate case," Appl. Opt. **57**(5), 1159–1167 (2018).
32. R. Ossikovski, M. Anastasiadou, S. Ben Hatit, E. Garcia-Caurel, and A. De Martino, "Depolarizing Mueller matrices: how to decompose them?" Phys. Status Solidi A **205**(4), 720–727 (2008).
33. L. Martin, G. Le Brun, and B. Le Jeune, "Mueller matrix decomposition for biological tissue analysis," Opt. Commun. **293**, 4–9 (2013).
34. R. Ossikovski and J. Vizet, "Eigenvalue-based depolarization metric spaces for Mueller matrices," J. Opt. Soc. Am. A **36**(7), 1173–1186 (2019).
35. A. Van Eeckhout, E. Garcia-Caurel, R. Ossikovski, A. Lizana, C. Rodríguez, E. González-Arnay, and J. Campos, "Depolarization metric spaces for biological tissues classification," J. Biophotoncis **13**(8), e202000083 (2020).
36. A. Van Eeckhout, A. Lizana, E. Garcia-Caurel, J. J. Gil, R. Ossikovski, and J. Campos, "Synthesis and characterization of depolarizing samples based on the indices of polarimetric purity," Opt. Lett. **42**(20), 4155–4158 (2017).
37. R. M. A. Azzam and N. M. Bashara, *Ellipsometry and Polarized Light* (North-Holland, 1977).
38. W. Lihong and V. W. Hsin, *Biomedical Optics, Principles and Imaging* (Wiley and Sons, 2007).

Biomedical Optics EXPRESS

39. W. Cheong, A. Welch, and S. Prahl, "A review of the optical properties of biological tissues," IEEE J. Quantum Electron. **26**(12), 2166–2185 (1990).
40. C. Rodriguez, A. Van Eeckout, E. Garcia-Caurel, J. Gil, T. Garnatje, E. Gonzalez-Arnay, J. Vidal, J. Escaler, I. Moreno, J. Campos, and A. Lizana, "Indices of Polarimetric Purity: application in biological tissues," Proc. SPIE **11646**, 116460P (2021).
41. A. Van Eeckhout, E. Garcia-Caurel, T. Garnatje, J. Escaler, M. Durfort, J. Vidal, J. Gil, J. Garcia-Romero, R. Ossikovski, I. Moreno, J. Campos, and A. Lizana, "Retrieving physical information of depolarizing systems," Proc. SPIE **11646**, 116460K (2021).
42. J. Gil and E. Bernabeu, "Depolarization and polarization indices of an optical system," Opt. Acta **33**(2), 185–189 (1986).
43. L. Sobin, M. Gospodarowicz, and C. Wittekind, *TNM Classification of Malignant Tumors*, 7th Edition (John Wiley & Sons, Inc., 2009).
44. N. Nishizawa, B. Al-Qadi, and T. Kuchimaru, "Angular optimization for cancer identification with circularly polarized light," J. Biophotonics **14**(3), e202000380 (2021).
45. T. Novikova, A. Pierangelo, A. De Martino, A. Benali, and P. Validire, "Polarimetric imaging for cancer diagnosis and staging," Opt. Photonics News **23**(10), 26–32 (2012).
46. G. Tjin, P. Xu, S. Kable, E. P. W. Kable, and J. K. Burgess, "Quantification of collagen I in airway tissues using second harmonic generation," J. Biomed. Opt. **19**(3), 036005 (2014).
47. T. Hompland, A. Erikson, M. Lindgren, T. Lindmo, and C. Davies, "Second-harmonic generation in collagen as a potential cancer diagnostic parameter," J. Biomed. Opt. **13**(5), 054050 (2008).
48. M. Borovkova, A. Popov, A. Bykov, and I. Meglinski, "Role of scattering and birefringence in phase retardation revealed by locus of Stokes vector on Poincaré sphere," J. Biomed. Opt. **25**(5), 057001 (2020).
49. M. Borovkova, A. Bykov, A. Popov, A. Pierangelo, T. Novikvoa, J. Pahnke, and I. Meglinski, "Evaluating β-amyloidosis progression in Alzheimer's disease with Mueller polarimetry," Biomed. Opt. Express **11**(8), 4509–4519 (2020).